

ON THE NUMBER OF STATIONARY PATTERNS IN REACTION-DIFFUSION SYSTEMS

Vojtěch Rybář, Tomáš Vejchodský

Institute of Mathematics, Czech Academy of Sciences
Žitná 25, Prague 1, 115 67, Czech Republic
{rybar,vejchod}@math.cas.cz

Abstract: We study systems of two nonlinear reaction-diffusion partial differential equations undergoing diffusion driven instability. Such systems may have spatially inhomogeneous stationary solutions called Turing patterns. These solutions are typically non-unique and it is not clear how many of them exists. Since there are no analytical results available, we look for the number of distinct stationary solutions numerically. As a typical example, we investigate the reaction-diffusion system designed to model coat patterns in leopard and jaguar.

Keywords: diffusion driven instability, Turing patterns, classification of non-unique solutions

MSC: 35A02, 35K57, 35Q92

1. Introduction

Nonlinear systems of reaction-diffusion equations are universally recognized instruments for modelling various phenomena in chemistry, biology, and ecology. Their popular applications include, but are not limited to, symmetry breaking, biochemical reactions, tumour vascularization, predator-prey models or skin and coat patterns in animals.

Research of the diffusion driven instability initiated Alan Turing in 1952 by his seminal paper [13], where he presented a counter-intuitive property of systems of two reaction-diffusion equations of the form

$$\frac{\partial u}{\partial t} = D_1 \Delta u + f(u, v) \quad \text{in } (0, \infty) \times \Omega, \quad (1)$$

$$\frac{\partial v}{\partial t} = D_2 \Delta v + g(u, v) \quad \text{in } (0, \infty) \times \Omega, \quad (2)$$

where $u = u(t, x)$, $v = v(t, x)$ correspond to concentrations of two chemical species, the domain $\Omega \subset \mathbb{R}^2$ models a chemical reactor, D_1, D_2 are diffusion coefficients

and $f(u, v)$, $g(u, v)$ are nonlinear reaction terms representing chemical reactions. We assume existence of constants $u_s, v_s \in \mathbb{R}$ such that $f(u_s, v_s) = g(u_s, v_s) = 0$. Clearly, these constants form a stationary solution of system (1)–(2) known as the ground state. In addition, these constants can be seen as a solution to the system of ordinary differential equations (ODE) coming from (1)–(2) for $D_1 = D_2 = 0$. Turing demonstrated that if u_s, v_s is a linearly stable uniform stationary solution of this ODE system then u_s, v_s seen as a solution to system (1)–(2) can become unstable for $D_1 \neq 0$, $D_2 \neq 0$ and its small spatially inhomogeneous perturbations may evolve to an inhomogeneous steady state. Such steady state is known as Turing pattern. However, the diffusion driven instability can occur only for a limited set of values of D_1 and D_2 and possible other parameters of (1)–(2). These values can be identified by means of the well known linear analysis, see e.g. [7].

There is a number of models exhibiting the diffusion driven instability and Turing patterns. For example, Thomas model [11] of substrate inhibition, Schnakenberg model [10] describing a hypothetical trimolecular reaction, Gray and Scott model [3] for an autocatalytic reaction in a tank reactor, BMA model [1] for symmetry breaking in morphogenesis and LLM model [5] for pigment pattern generation on coats of leopards and jaguars.

The mentioned linear analysis describes well the initial evolution of small perturbations of the ground state, but it yields no information about their development if they grow sufficiently large. Existing analytical results about solutions farther away from the ground state are limited. Therefore, we study them numerically. We are then limited to an empirical study of a particular case only, but we aim to collect a large amount of data, process them by statistical methods and draw more general conclusions.

In this contribution we present results of a particular numerical study focused on the number of distinct Turing patterns in the LLM model [5]. In this experiment we initiated the evolution with several thousand distinct initial conditions, solve them by a fast numerical scheme, and postprocess the obtained results by nontrivial methods to identify patterns that are identical up to natural symmetries of the problem. The following section introduces periodic boundary conditions and the corresponding symmetries of the problem. Section 3 briefly describes the spectral Fourier method. Section 4 introduces the LLM model, its particular setting, and explains how the computed results are postprocessed and analysed. Section 5 presents the obtained results, especially the numbers of distinct equivalence classes of stationary solutions. Finally, Section 6 draws conclusions and offers prospects for further research.

2. Boundary conditions and problem symmetries

Within this paper, we consider the domain Ω to be a square $\Omega = (0, L)^2$. The reaction-diffusion system (1)–(2) is usually equipped with no flux boundary conditions. However, we will consider periodic boundary conditions, because they are

natural for the spectral Fourier method, which we will use below. In particular, we consider these periodic boundary conditions:

$$u(0, y) = u(L, y) \quad \forall y \in (0, L) \quad \text{and} \quad u(x, 0) = u(x, L) \quad \forall x \in (0, L), \quad (3)$$

$$v(0, y) = v(L, y) \quad \forall y \in (0, L) \quad \text{and} \quad v(x, 0) = v(x, L) \quad \forall x \in (0, L), \quad (4)$$

$$\partial_x u(0, y) = \partial_x u(L, y) \quad \forall y \in (0, L) \quad \text{and} \quad \partial_y u(x, 0) = \partial_y u(x, L) \quad \forall x \in (0, L), \quad (5)$$

$$\partial_x v(0, y) = \partial_x v(L, y) \quad \forall y \in (0, L) \quad \text{and} \quad \partial_y v(x, 0) = \partial_y v(x, L) \quad \forall x \in (0, L). \quad (6)$$

Since the square domain and these periodic boundary conditions are invariant with respect to mirroring and rotations by $\pi/2$, we show that the stationary solutions of problem (1)–(2) with boundary conditions (3)–(6) possess the same symmetries. To be rigorous, we define the mirror image of a function u defined in Ω by

$$\bar{u}(x, y) = u(L - x, y). \quad (7)$$

Similarly, we define a function rotated by $\pi/2$ (counter-clockwise) as

$$\hat{u}(x, y) = u(L - y, x). \quad (8)$$

Further, the periodic boundary conditions enable to shift a stationary solution periodically in such a way that it remains a stationary solution. To be precise, we define a periodic shift of a function u by a vector $(r, s) \in (0, L)^2$ as

$$\tilde{u}(x, y) = \begin{cases} u(x + r, y + s) & \text{for } x \in (0, L - r), y \in (0, L - s), \\ u(x + r, y + s - L) & \text{for } x \in (0, L - r), y \in (L - s, L), \\ u(x + r - L, y + s) & \text{for } x \in (L - r, L), y \in (0, L - s), \\ u(x + r - L, y + s - L) & \text{for } x \in (L - r, L), y \in (L - s, L). \end{cases} \quad (9)$$

Lemma 1. *Let $u, v \in C^2(\Omega) \cap C^0(\bar{\Omega})$ form a stationary solution to problem (1)–(2) with boundary conditions (3)–(6). Then both pairs of functions \bar{u}, \bar{v} and \hat{u}, \hat{v} defined by (7) and (8), respectively, are stationary solutions to (1)–(2) with (3)–(6) as well. Moreover, if the shifted functions \tilde{u}, \tilde{v} given by (9) with arbitrary $(r, s) \in (0, L)^2$ are both in $C^2(\Omega)$ then they again form a stationary solution to (1)–(2) with (3)–(6).*

Proof. It is easy to verify that all \bar{u}, \bar{v} and \hat{u}, \hat{v} are in $C^2(\Omega) \cap C^0(\bar{\Omega})$ and that they satisfy the periodic boundary conditions (3)–(6). Further, let $(x, y) \in \Omega$. Then it is easy to see that $\Delta \bar{u}(x, y) = \Delta u(L - x, y)$, $\Delta \hat{u}(x, y) = \Delta u(L - y, x)$, and similarly for \bar{v} and \hat{v} . Since u, v satisfy equations (1)–(2) at both points $(L - x, y) \in \Omega$ and $(L - y, x) \in \Omega$, we conclude that both pairs \bar{u}, \bar{v} and \hat{u}, \hat{v} satisfy the same equations at (x, y) .

Concerning the shifted functions \tilde{u}, \tilde{v} we may proceed in the same way. The only difficulty is the fact that the periodic shift \tilde{u}, \tilde{v} need not automatically be in $C^2(\Omega)$ and therefore the additional assumption is needed. \square

3. Spectral Fourier collocation method

To solve problem (1)–(2) with periodic boundary conditions (3)–(6) efficiently, we employ the spectral Fourier collocation method [4, 12]. In order to briefly introduce the main idea of the method, we consider a 2π -periodic function $z(x)$ sampled on the spatial discretization grid $x_j = 2\pi j/N$ with $z_j = z(x_j)$, $j = 0, 1, 2, \dots, N$. Note that we consider N to be even for simplicity. By periodicity of $z(x)$ we have $z_0 = z_N$. Using the discrete Fourier transform (DFT) and the inverse discrete Fourier transform (IDFT), both properly defined and discussed in [12], we can compute the derivatives $w_j = z'(x_j)$, $j = 1, \dots, N$, by the following procedure:

1. Compute the DFT $\hat{z}_k = (2\pi/N) \sum_{j=1}^N \exp(-ikx_j) z_j$, $k = -N/2 + 1, \dots, N/2$.
2. Set $\hat{w}_k = ik\hat{z}_k$, $k = -N/2 + 1, \dots, N/2$.
3. Compute the IDFT $w_j = (1/(2\pi)) \sum_{k=-N/2+1}^{N/2} \exp(ikx_j) \hat{w}_k$, $j = 1, \dots, N$.

Similarly, the second derivative $w_j = z''(x_j)$ can be computed by the same procedure, but item 2 has to be replaced by $\hat{w}_k = -k^2 \hat{z}_k$, $k = -N/2 + 1, \dots, N/2$.

This idea can be easily applied in two dimensions as well. Let us consider partitions $x_m = 2\pi m/N$ and $y_n = 2\pi n/N$, $m, n = 1, 2, \dots, N$, of $[0, 2\pi]$ corresponding to x and y directions. Set $u_{m,n} = u(x_m, y_n)$, $v_{m,n} = v(x_m, y_n)$, $f_{m,n} = f(u_{m,n}, v_{m,n})$, and $g_{m,n} = g(u_{m,n}, v_{m,n})$. The two-dimensional DFT of $u_{m,n}$ is defined as

$$\hat{u}_{k,\ell} = \frac{4\pi^2}{N^2} \sum_{m=1}^N \sum_{n=1}^N \exp(-i(kx_m + \ell y_n)) u_{m,n}, \quad k, \ell = -N/2 + 1, \dots, N/2, \quad (10)$$

and similarly for $\hat{v}_{k,\ell}$, $\hat{f}_{k,\ell}$, and $\hat{g}_{k,\ell}$. Correspondingly, the two-dimensional IDFT of $\hat{u}_{k,\ell}$ is

$$u_{m,n} = \frac{1}{4\pi^2} \sum_{k=-N/2+1}^{N/2} \sum_{\ell=-N/2+1}^{N/2} \exp(i(kx_m + \ell y_n)) \hat{u}_{k,\ell}, \quad m, n = 1, 2, \dots, N. \quad (11)$$

In order to use the DFT (10) for equations (1) and (2), we first transform variables to map $[0, L]$ into $[0, 2\pi]$ and then we obtain the following system of ordinary differential equations for the Fourier images $\hat{u}_{k,\ell}$ and $\hat{v}_{k,\ell}$:

$$\frac{d\hat{u}_{k,\ell}}{dt} = -D_1 \frac{4\pi^2}{L^2} (k^2 + \ell^2) \hat{u}_{k,\ell} + \hat{f}_{k,\ell} \quad k, \ell = -N/2 + 1, \dots, N/2, \quad (12)$$

$$\frac{d\hat{v}_{k,\ell}}{dt} = -D_2 \frac{4\pi^2}{L^2} (k^2 + \ell^2) \hat{v}_{k,\ell} + \hat{g}_{k,\ell} \quad k, \ell = -N/2 + 1, \dots, N/2. \quad (13)$$

Here, $\hat{f}_{k,\ell}$ and $\hat{g}_{k,\ell}$ are computed by the DFT (10) from $f_{m,n} = f(u_{m,n}, v_{m,n})$ and $g_{m,n} = g(u_{m,n}, v_{m,n})$, where the values of $u_{m,n}$ and $v_{m,n}$ have to be computed from the Fourier images $\hat{u}_{k,\ell}$ and $\hat{v}_{k,\ell}$ by the IDFT (11).

In order to solve the system of ordinary differential equations (12) efficiently, we utilize the fourth order Runge-Kutta method as in [4] and the fast Fourier transform.

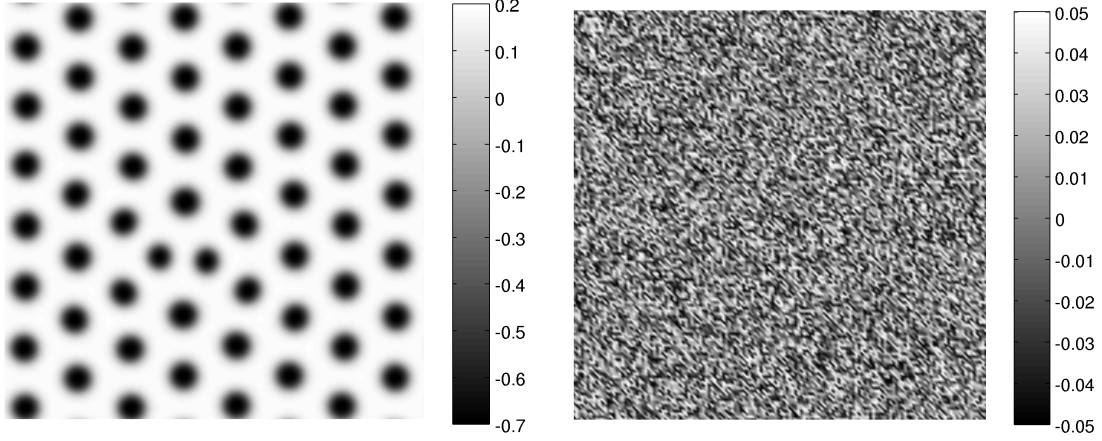


Figure 1: The left panel shows the component v of the stationary solution of problem (14)–(15) with periodic boundary conditions (3)–(6) as it evolved from a small random initial condition illustrated in the right panel.

4. Problem setting and postprocessing of results

For the numerical study presented below, we will consider the LLM model [5]. It consists of the following reaction-diffusion system:

$$\frac{\partial u}{\partial t} = D\delta\Delta u + \alpha u + v - r_2 uv - \alpha r_3 uv^2, \quad (14)$$

$$\frac{\partial v}{\partial t} = \delta\Delta v - \alpha u + \beta v + r_2 uv + \alpha r_3 uv^2 \quad (15)$$

with $D = 0.45$, $\delta = 6$, $\alpha = 0.899$, $\beta = -0.91$, $r_2 = 2$, and $r_3 = 3.5$. These parameter values yield stationary solutions that correspond to spotted patterns, see Figure 1 (left) for a typical pattern and Figure 1 (right) for the corresponding initial condition. Our main interest is to find how many different patterns can evolve from small random initial conditions. Note that the two components u and v are complementary to each other in the sense that local maxima of u correspond to local minima of v . Therefore, we concentrate on the component v only in what follows.

All patterns in this paper including Figure 1 are computed by the spectral Fourier collocation method with the following setting. The domain is a square $\Omega = (0, L)^2$ with $L = 200$. The discretization grid contains $N = 144$ points in every direction. Initial conditions are generated as a uniformly distributed random number within $(-0.05, 0.05)$ for every node of the grid. These initial conditions mimic small amplitude random fluctuations around the spatially homogeneous steady state. The time step of the fourth order Runge-Kutta method is chosen as $\Delta t = 1$ and the computation of the time evolution is terminated as soon as the relative difference of approximate solutions at two consecutive time steps is smaller than a prescribed tolerance. In particular, if $\|\cdot\|_{l^2}$ stands for the l^2 -norm over the grid nodes and $v^{(k)}$

and $v^{(k+1)}$ denote the solution at times $t_k = k\Delta t$ and $t_{k+1} = (k+1)\Delta t$, then the computation is stopped if

$$\frac{\|v^{(k)} - v^{(k+1)}\|_{l^2}}{\|v^{(k)}\|_{l^2}} < 10^{-4}. \quad (16)$$

Using this setting, we generated a number of random initial conditions and computed the corresponding stationary solutions. However, based on the symmetries of the stationary solutions described in Lemma 1, each stationary solution represents a whole class of solutions equivalent up to one of the transformations (7)–(9). Therefore, finding the number of distinct stationary solutions, i.e. solutions that are not equivalent in the sense of transformations (7)–(9), is a nontrivial task. Especially challenging is the fact that any shift $(r, s) \in (0, L)^2$ yields a stationary solution and, hence, each class of solutions is uncountable.

5. Results

In total we computed stationary solutions for 5297 different random initial conditions. At first, we calculate the number of spots in each of these patterns. To compute this number we plot the v component of the given pattern as a bitmap image and utilize the Matlab Image Processing Toolbox [6]. In particular, we use the function `imfindcircles` which seeks circles in a given image and returns coordinates of their centres and radii. The number of spots is then simply equal to the number of returned centres. Having computed this number for all patterns, we then simply calculate how many patterns have a given number of spots. Figure 2 presents these data in the form of a histogram.

In this histogram we identify 15 possible numbers of spots. Number of spots varies between 50 and 65 with the intermediate numbers being naturally the most frequent. Surprising is the relatively wide range of these numbers. Researchers have usually a chance to observe a relatively small amount of patterns and then they tend to conclude that the number of spots is (almost) constant for the given parameter values and the size of the domain. However, our results show that it may vary considerably just due to the random variations in the initial condition. In this particular case, the variation in the number of spots is up to $\pm 15\%$.

Nevertheless, the main goal is to find the number of classes of solutions that are identical up to a combination of transformations (7)–(9). The computed number of spots serves as a first filter, because, clearly, if two patterns have a different number of spots, they cannot be equivalent. Thus, we split all patterns into 15 sets according to the number of spots and for each set we find classes of equivalent patterns as follows.

We keep a database of classes. Each class in this database is determined by one representative pattern. Initially the database is empty and the first pattern from the investigated set is chosen as the representative of the first class. Then for each pattern in the set, we find if it is equivalent to one of the stored representatives in the

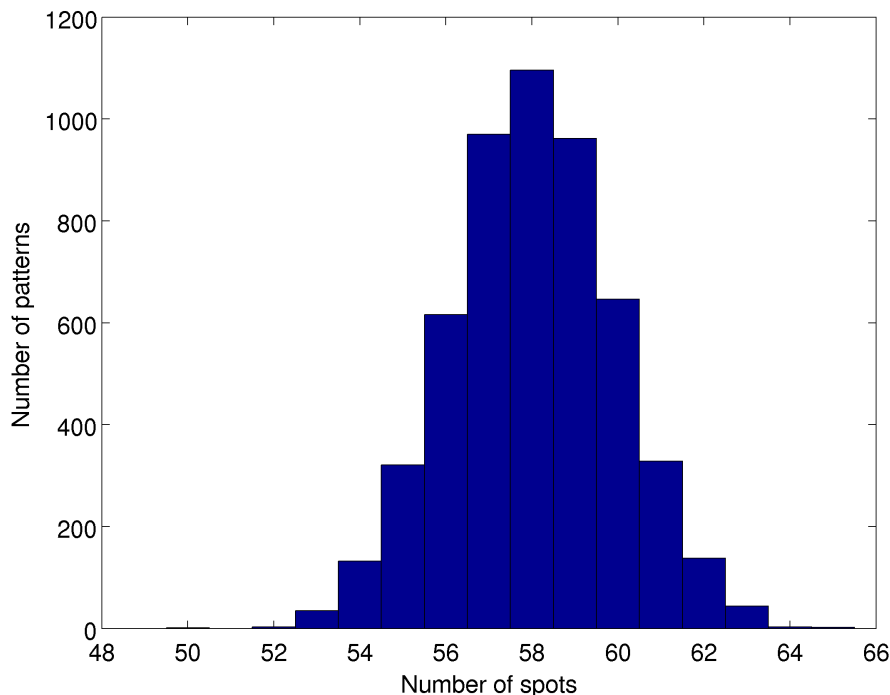


Figure 2: Distribution of the number of spots in stabilized patterns

database. If it is the case, we simply increase the counter of the number of patterns in the corresponding class. If not, then this pattern becomes a representative of a new class. As soon as we exhaust the entire investigated set of patterns, all classes of equivalent patterns are identified.

The important step in this algorithm is to decide whether a pattern is equivalent to a representative or not. In order to decide, we have to test all eight independent combinations of mirroring (7) and rotation (8) as well as all possible shifts (9). Fortunately, only the shifts that map a spot of the pattern to a spot of the representative are relevant and thus the total number of relevant shifts is finite and equals to the number of possible pairs of spots. If the number of spots in both the pattern and in the representative is n then the number of possible shifts is n^2 .

The crucial operation here is the comparison of two patterns – the transformed pattern and the representative – and the decision whether they match or not. The point is that exact equality of two patterns cannot work here, because the patterns are polluted by various numerical errors. Therefore, we actually look for patterns matching up to a certain precision. We experimented with several measures and we obtained the best results by using the modified Hausdorff distance on the torus for the computed centres of spots. Note that the torus topology comes from the periodic boundary conditions (3)–(6).

The modified Hausdorff distance $\tilde{H}(A, B)$ in the torus is defined as

$$\tilde{H}(A, B) = \min \left\{ \tilde{h}(A, B), \tilde{h}(B, A) \right\},$$

where $\tilde{h}(A, B)$ is the Hausdorff distance expressing the maximal distance between points from the set A to the set B , i.e.

$$\tilde{h}(A, B) = \max_{a \in A} \left\{ \min_{b \in B} \tilde{d}(a, b) \right\},$$

where $\tilde{d}(a, b)$ is the torus distance of points $a = (a_1, a_2)$ and $b = (b_1, b_2)$:

$$\tilde{d}(a, b) = \left(\min\{|a_1 - b_1|, L - |a_1 - b_1|\}^2 + \min\{|a_2 - b_2|, L - |a_2 - b_2|\}^2 \right)^{1/2}.$$

We use the modified Hausdorff distance rather than the Hausdorff distance itself, because it is symmetric and performs better [2]. In order to gain the required efficiency we use the Matlab mex-file implementation of the modified Hausdorff distance [9].

Using the modified Hausdorff distance on the torus, we compare two patterns based on the lists C_1 and C_2 of coordinates of centres of their spots. We simply compute $\tilde{H}(C_1, C_2)$ and test if it is below a chosen threshold. To be precise, we have to consider also the transformations (7)–(9). The two patterns to compare are determined by the lists C_1 and C_2 of their centres of spots. For the list C_1 , we consider all its shifts (9) with $(r, s) = (b_1 - a_1, b_2 - a_2)$ for all $(a_1, a_2) \in C_1$ and all $(b_1, b_2) \in C_2$ together with eight possible combinations of mirroring (7) and rotations (8). Denoting the set of all these transformations by \mathcal{R} , we compute

$$\tilde{H}(C_1, C_2) = \min_{\rho \in \mathcal{R}} \tilde{H}(\rho(C_1), C_2), \quad (17)$$

where $\rho(C_1)$ stands for the transformation of the set C_1 .

Practically, we have chosen the above mentioned threshold to be 0.75 and consider two patterns to match if $\tilde{H}(C_1, C_2) < 0.75$. However, we have to admit that the choice of this threshold is delicate, because it is difficult to distinguish whether two patterns differ due to numerical errors or whether they really correspond to different stationary solutions. For illustration, we present Figure 3 showing two sets of centres of spots with the distance $\tilde{H}(C_1, C_2) \approx 0.74941$.

The final results are summarized in Table 1, where we identified the number of distinct classes of stationary solutions. We observe that the number of these classes varies roughly between 10 and 20 % of the total number of patterns in each set with a higher number of spots. This ratio is naturally higher in the rare cases where the number of identified patterns is low.

An interesting observation is that there are considerably different numbers of distinct classes for pairs of sets with comparable total numbers patterns. See for example the cases of 56 and 60 spots, which both have slightly above 600 patterns, but the first case has only 67 distinct classes of solutions in contrast to 96 classes in the second case.

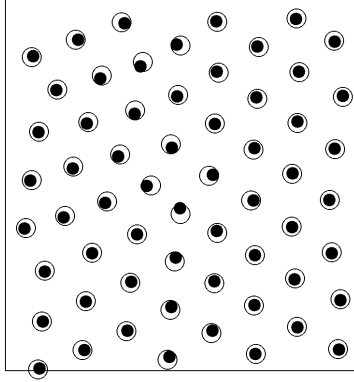


Figure 3: Centres of spots of two patterns with $\tilde{H}(C_1, C_2) \approx 0.74941$

Spots	50	52	53	54	55	56	57	58	59	60	61	62	63	64	65
Patterns	1	3	35	132	321	616	970	1096	962	646	328	138	44	3	2
Classes	1	3	6	22	34	67	70	123	115	96	34	27	20	3	2

Table 1: Number of classes for different number of spots in patterns

6. Conclusions

The results presented in Table 1 are especially interesting if they are compared with our previous results [8], where we performed a similar study, but for much smaller domain, namely, $\Omega = (0, 50)^2$. In that case, we obtained only two different numbers of spots and in total four distinct classes of solutions out of 6 000 computed patterns. In view of these results, the variety in both the number of spots and the number of classes of patterns we observe in Table 1 is rather surprising, even if we take into account the larger size of the domain Ω . These results strongly indicate that the number of distinct classes of patterns as well as the possible number of spots grow progressively with the size of the domain Ω .

Another observation is that the influence of boundary conditions on the final shape of the pattern is smaller if the domain is larger. Therefore, in the older study [8] we observe mainly the effects of boundary conditions, while in the current study we see mostly the natural variability of Turing patterns with the influence of boundary conditions being inferior.

Clearly, the presented results are burdened by uncertainties. For example, it is difficult to verify whether the numerical process of computing the stationary solution really converged. Even if the stopping criterion (16) is fulfilled, the pattern still might not be completely stationary. As a result, we can identify two patterns as distinct, but they both can eventually converge to the same stationary solution. This effect could hypothetically contribute to the observed high number of distinct classes of solutions.

Moreover, we obviously did not find all the possible classes of patterns. Particularly odd is the fact that we found classes with 50 and 52 spots, but none with 51 spots. Due to the nature of the problem, we believe that such patterns exist and that we just did not capture the rare stationary solutions. An experiment with a larger sample of computed patterns could help to estimate how many of these rare solutions we missed.

In the current numerical study we focused on the particular LLM model [5], but as a future project we plan to perform a similar study for other models. For example for the Thomas model [11]. Based on our experience, we expect that if we chose the problem parameters in such a way that the number of spots is similar to the current study, we obtain similar results.

Further, the obtained results can help us to understand additional subtle features of Turing patterns. For example, we can try to identify the natural period of the Turing patterns as a natural distance between two spots. This task can be accomplished by numerical methods and the results can help to find an analytical expression or estimate of the period and prove a corresponding theoretical result.

Acknowledgements

This work has been supported by grant SVV-2015-260226 of the Charles University Grant Agency and by RVO 67985840.

References

- [1] Barrio, R., Maini, P., and Aragón, J.: Size-dependent symmetry breaking in models for morphogenesis. *Physica D* **2920** (2002), 1–12.
- [2] Dubuisson, M.P. and Jain, A.K.: A modified Hausdorff distance for object matching. In: *Proc. of IAPR Int. Conf. on Pattern Recognition*, pp. A:566–568. Jerusalem, Israel, 1994.
- [3] Gray, P. and Scott, S.: Autocatalytic reactions in the isothermal, continuous stirred tank reactor. *Chem. Eng. Sci.* **39** (1984), 1087–1097.
- [4] Kassam, A.K.: Solving reaction-diffusion equations 10 times faster. Numerical Analysis Group Research Report **16** (Mathematical Institute, Oxford, 2003).
- [5] Liu, R. T., Liaw, S. S., and Maini, P. K.: Two-stage Turing model for generating pigment patterns on the leopard and the jaguar. *Physical Review* **74** (2006), 011 914.
- [6] MATLAB: *Image Processing Toolbox 2014b*. The MathWorks Inc., Natick, Massachusetts, United States, 2014.
- [7] Murray, J. D.: *Mathematical biology. II. Spatial models and biomedical applications*. Springer-Verlag, New York, 2003.

- [8] Rybář, V. and Vejchodský, T.: Variability of Turing patterns in reaction-diffusion systems. In: H. Bílková, M. Rozložník, and P. Tichý (Eds.), *Proceedings of the SNA '14*, pp. 87–90. Institute of Computer Science AS CR, Prague, 2014.
- [9] Sasikanth, B.: Modified Hausdorff distance for 2D point sets. <https://www.mathworks.com/matlabcentral/fileexchange/30108>. Accessed 2015-05-25.
- [10] Schnakenberg, J.: Simple chemical reaction systems with limit cycle behaviour. *J. Theoret. Biol.* **81** (1979), 389–400.
- [11] Thomas, D.: Artificial enzyme membranes, transport, memory, and oscillatory phenomena. In: D. Thomas and J.P. Kernevez (Eds.), *Analysis and control of immobilized enzyme systems*, pp. 115–150. North Holland, Amsterdam, 1976.
- [12] Trefethen, L.N.: *Spectral methods in MATLAB*. SIAM, Philadelphia, 2000.
- [13] Turing, A.M.: The chemical basis of morphogenesis. *Philosophical Transactions of the Royal Society B* **237** (1952), 37–72.